Published in final edited form as:

J Mol Cell Cardiol. 2019 May ; 130: 160–169. doi:10.1016/j.yjmcc.2019.04.006.

Drp1/Fis1 Interaction Mediates Mitochondrial Dysfunction in Septic Cardiomyopathy

Bereketeab Haileselassie[1,2], **Riddhita Mukherjee**[1,2], **Amit U. Joshi**[2], **Brooke A. Napier**[3], **Liliana M. Massis**[3], **Nicolai Patrick Ostberg**[2], **Bruno B. Queliconi**[2], **Denise Monack**[3], **Daniel Bernstein**[1], **Daria Mochly-Rosen**[2]

[1]Department of Pediatrics; Stanford University School of Medicine; Stanford, CA 94305; USA

[2]Department of Chemical and Systems Biology; Stanford University School of Medicine; Stanford, CA 94305; USA

[3]Department of Microbiology; Stanford University School of Medicine; Stanford, CA 94305; USA

Abstract

Mitochondrial dysfunction is a key contributor to septic cardiomyopathy. Although recent literature implicates dynamin related protein 1 (Drp1) and its mitochondrial adaptor fission 1 (Fis1) in the development of pathologic fission and mitochondrial failure in neurodegenerative disease, little is known about the role of Drp1/Fis1 interaction in the context of sepsis-induced cardiomyopathy. Our study tests the hypothesis that Drp1/Fis1 interaction is a major driver of sepsis-mediated pathologic fission, leading to mitochondrial dysfunction in the heart.

Methods: H9C2 cardiomyocytes were treated with lipopolysaccharide (LPS) to evaluate changes in mitochondrial membrane potential, oxidative stress, cellular respiration, and mitochondrial morphology. Balb/c mice were treated with LPS, cardiac function was measured by echocardiogaphy, and mitochondrial morphology determined by electron microscopy (EM). Drp1/Fis1 interaction was inhibited by P110 to determine whether limiting mitochondrial fission can reduce LPS-induced oxidative stress and cardiac dysfunction.

Results: LPS-treated H9C2 cardiomyocytes demonstrated a decrease in mitochondrial respiration followed by an increase in mitochondrial oxidative stress and a reduction in membrane potential. Inhibition of Drp1/Fis1 interaction with P110 attenuated LPS-mediated cellular oxidative stress and preserved membrane potential. In vivo, cardiac dysfunction in LPS-treated mice was associated with increased mitochondrial fragmentation. Treatment with P110 reduced cardiac mitochondrial fragmentation, prevented decline in cardiac function, and reduced mortality.

Submission and corresponding author: Bereketeab Haileselassie M.D, M.H. S, Stanford University, School of Medicine, Division of Pediatric Critical Care, 770 Welch Road, Suite 435, Palo Alto, CA 94304, Phone: 301-580-4167, bhailes3@stanford.edu.

Contributions: B.H., D.B., D.M. and D.M.R. generated the hypothesis and experimental design. B.H. and R.M. prepared the manuscript. R.M., A.U.J, B.A.N., L.M.M., N.O. and B.H. conducted experiments and helped with data analysis. All the authors reviewed and edited the manuscript.

Conflict of interest: Patents on P110 and its utility in HD and other neurodegenerative diseases have been filed by D.M-R and A.U.J, and were licensed to Mitoconix Bioscience, a company that D.M-R founded and serves on its board. However, none of the work in her laboratory was carried out in collaboration with or with financial support from the company. A.U.J advised the company, as part of technology transfer agreement, on his work related to Huntington's disease. The other authors declare that they have no conflict of interest.

Conclusions: Sepsis decreases cardiac mitochondrial respiration and membrane potential while increasing oxidative stress and inducing pathologic fission. Treatment with P110 was protective in both *in vitro* and *in vivo* models of septic cardiomyopathy, suggesting a key role of Drp1/Fis1 interaction, and a potential target to reduce its morbidity and mortality.

Keywords

Sepsis; heart failure; mitochondrial fission; Drp1

1. Introduction

Sepsis continues to be a major cause of morbidity and mortality as well as a substantial financial burden worldwide (1). This is evident by the increasing prevalence of sepsis and septic shock over the last two decades (1, 2). In the progression of sepsis-induced multi-organ dysfunction syndrome (MODS), the role of septic cardiomyopathy is becoming increasingly apparent, with data showing an association between mortality and cardiac dysfunction in sepsis (4). Whereas the significance of cardiac failure in sepsis-induced mortality is well described, the mechanisms behind cardiac dysfunction in sepsis remains elusive (5).

Recent focus on “cytopathic hypoxia”, a disturbance of cellular bioenergetics in sepsis, has revealed the influence of mitochondrial oxidative stress on multi-organ system failure and mortality (6,7). Enhanced production of mitochondrial reactive oxygen species (ROS) in sepsis induces peroxidation of the mitochondrial lipid cardiolipin, leading to release of cytochrome c and activation of cell death pathways (8,9). Furthermore, several clinical studies have demonstrated alterations in mitochondrial respiration and decreased mitochondrial content in peripheral blood mononuclear cells (PBMCs) is associated with illness severity and mortality (10,11).

An underexplored mechanism in the development of myopathy in sepsis is that of alterations in mitochondrial dynamics (fission, fusion, and mitophagy), resulting in oxidative stress and mitochondrial dysfunction (12). Under physiological conditions, mitochondria are maintained in dynamic networks, which result from the opposing processes of fusion and fission. Fusion is regulated by mitochondria-associated optical atrophy 1 (OPA1) and mitofusins 1 and 2 (MFN1 and MFN2), whereas fission is regulated by dynamin-related protein 1 (Drp1) through its interactions with mitochondrial adaptors including fission 1 (Fis1), mitochondrial fission factor (Mff) and mitochondrial dynamics proteins 49 and 51 (Mid49 and 51) (13). Drp1 is predominantly cytosolic under basal conditions, but upon activation, Drp1 oligomerizes and is recruited to the mitochondrial surface where it binds to the above mitochondrial adaptors to assemble the infrastructure required for mitochondrial fission (12,13). Whereas physiologic levels of fission are necessary for mitochondrial quality control, excessive mitochondrial fission/fragmentation leads to decreased mitochondrial function and increased oxidative stress (13,14).

To further elucidate the role of individual mitochondrial adaptors in Drp1 recruitment, our laboratory has developed adaptor-specific inhibitors of Drp1/Fis1 interaction (P110) as well as Drp1/Mff interaction (P259) (15,13). Results from previous work have demonstrated that

selective inhibition of the Drp1/Fis1 interaction abrogates pathologic fragmentation in neurodegenerative disease and cardiac injury models while having no effect under physiological conditions (14,15). In contrast, blocking Drp1/Mff interaction, using peptide P259, results in elongated mitochondria and disruption of mitochondrial function under basal conditions, and hastens disease progression in a mouse model of Huntington's disease (13).

Whereas the role of mitochondrial dynamics has been well described in neurodegenerative disease and myocardial ischemia, its significance in the setting of sepsis-induced multi-organ dysfunction syndrome and septic cardiomyopathy is unknown. Thus, using both cardiomyocyte and animal models of sepsis, we demonstrate increasing mitochondrial fragmentation that is Drp1/Fis1-dependent in sepsis-induced myocardial dysfunction. Furthermore, we show Drp1/Fis1-dependent mitochondrial fragmentation is linked with derangements in oxidative stress and mitochondrial respiration as well as cell death. Importantly, we demonstrate that inhibition of Drp1/Fis1 interaction by P110 attenuates pathological fission and subsequent mitochondrial dysfunction leading to improved cardiac function and improves survival in sepsis.

2. Materials and Methods

2.1. Cell Line and Animals

H9C2 cardiomyocytes were cultured in DMEM supplemented with 10% FBS, 4 mM glutamine, 100 U/ml penicillin, 10 μg/ml streptomycin in a 5% CO_2 incubator at 37°C.

All animal experiments were carried out under the protocols (APLAC-33002) approved by the Institutional Animal Care and Use Committee of Stanford University. 4–6-week old female BALB/c mice were ordered from Jackson laboratory (Bar-Harbor, Maine). After one week of acclimation, the mice were utilized for the LPS model of sepsis at the age of 5–7 weeks.

2.2. Peptides

Drp1/Fis1 interaction peptide inhibitor, P110 (16), Drp1/Mff interaction peptide inhibitor, P259 (13) cross biological membranes due to their conjugation to the cell permeable peptide $TAT_{47–57}$. All peptides were synthesized by Ontores Biotechnologies (Hangzhou, China). The purity of peptides was > 90% measured by RP-HPLC chromatogram.

H9C2 cardiomyocytes were treated with P110 at a dose of 1 μM and P259 at a dose of 2 μM (17). P110 was injected to BALB/c mice at 0.5mg/kg/day (dissolved in 0.2 ml of saline) intraperitoneally, based on previous protocols (16). Control-and LPS-treated animals received 0.2 ml of saline daily to simulate a similar handling. P110 was dosed approximately 3 hours following LPS treatment to simulate the clinical presentation and timeline to treatment.

2.3. LPS Treatment: Cardiac Cell Line and Animal Model

2.3.a. H9C2 cardiomyocytes: H9C2 cardiomyocytes were seeded and allowed to attach overnight before treatment with LPS (0.5 μg/ml) from *E.coli* 0111:B4 (Sigma, lot #: 014M4019V).

2.3.b. Animal experiments: 7-week old BALB/c mice were randomized into control (n =15), LPS (n = 30), and a LPS + P110-treated groups (n = 30) groups. LPS was administered at 8 mg/kg to induce a severe sepsis phenotype. Following treatment, illness severity was followed using changes in body temperature, weight loss, and combined mouse sepsis scores (validated illness severity scoring system for murine sepsis model) (17).

2.4 Echocardiography:

Echocardiography was performed at 6, 12 and 24 hours after LPS treatment to attain ejection fraction (EF), fractional shortening (FS) and velocity time integral (VTI) across the left ventricular outflow tract. Transthoracic echocardiography was performed using the Vivid 7 platform (GE Medical Systems, Milwaukee, WI, USA). Two-dimensional, M-mode, and Doppler echocardiographic examinations were performed using a 13-MHz linear transducer. Two-dimensional imaging was acquired at a minimum depth setting of 2 cm and the images were adjusted to the heart size with the enhanced resolution imaging function. All M-mode and Doppler spectra are recorded at a sweep speed of 200 mm/sec for off-line analysis.

A subset of animals was sacrificed after 24 h (control (n =5), LPS (n = 10), LPS + P110 (n = 10)) for tissue analysis, while the rest of the mice were observed for 5 days to characterize illness severity and survival analysis.

2.5. Animal Illness severity:

Illness severity following LPS treatment was evaluated using a previously validated mouse sepsis score (17). The illness severity scoring system included a variety of subjective variables including: level of spontaneous activity, response to touch and auditory stimuli, posture, respiration rate and quality (labored breathing or gasping), and appearance (i.e. degree of piloerection). Each of these variables are given a score between 0 and 4, where 4 represents highest illness severity in each category (17). Mouse sepsis score was tabulated by a blinded observer on each of the animals every 3 hrs. for the first 24 hrs. Results were represented as a cumulative mouse sepsis score where we took the sum of the 24 hr. mouse sepsis scores for each animal.

2.6. Immunofluorescence for Mitochondrial Morphology

Cells cultured on a 96 well chamber were incubated with different treatment conditions (vehicle control, LPS or LPS+P110). Following treatment, cells were incubated with 66 nM Mitotracker Deep Red (Invitrogen, CA) and Hoechst (1: 10,000) for 20 minutes and images were acquired using an All-in-One Fluorescence Microscope BZ-X700 (Keyence). For time lapse imaging, cells were transfected with 100 ng Su9-EGFP per well using Lipofectamine 2000 (Invitrogen, CA). Two days after transfection, a time lapse was performed, imaging cells every two hours. Mitochondrial morphology was then quantified using a high throughput analysis script in MATLAB.

2.7. Cell and Mitochondrial Function Assays

2.7.a. Mitochondrial membrane potential: H9C2 cardiomyocytes were incubated with 50 nM tetra-methyl-rhodamine methyl ester (TMRM) (Invitrogen, CA) and Hoechst (1: 10,000) in HBSS (Hank's balanced salt solution) for 20 minutes at 37°C, as per the manufacturer's protocol. The fluorescence was analyzed on a SpectraMax M2e microplate reader (Molecular devices, CA) at excitation/emission maxima of 544/645 nm for TMRM and 350/470 nm for Hoechst, trihydrochloride trihydrate, staining. All data were normalized to (a) the number of cells per well, as quantified by total number of Hoechst + nuclei, and to (b) the TMRM fluorescence intensity of the control no-treatment cells.

2.7.b. ATP measurements: Adenosine triphosphate level was assayed by the ATP colorimetric/fluorometric assay kit (Biovision, Milpitas, CA) using the manufacturer's protocols. Fluorescence intensity was measured using SpectraMax M2e microplate reader (Molecular devices, CA).

2.7.c. ROS production: For total cellular ROS detection, H9C2 cardiomyocytes were incubated with 5 μM CellROX™ oxidative stress reagent (Invitrogen, CA) for 20 minutes along and co-stained with Hoechst at 37°C in the dark. The fluorescence was analyzed using SpectraMax M2e microplate reader (Molecular devices, CA), at excitation/emission maxima of 485/520 nm for CellROX™. Fluorescence intensity was then normalized for cell number (determined by Hoechst staining). For detection of mitochondrial ROS production, cells were treated with 5 μM MitoSOX™ Red, a mitochondrial superoxide indicator (Invitrogen, CA) for 20 minutes along with Hoechst staining at 37°C, according to the manufacturer's protocol, and fluorescence was analyzed at excitation/emission maxima of 510/588 nm.

2.7.d. Cellular respiration: Oxygen consumption rate (OCR) was measured with an XFe24 Extracellular Flux Analyzer (Seahorse Bioscience). Cells were seeded in an XF 24-well cell culture microplate at 40,000 cells per well (Seahorse Bioscience) in 250 μl of DMEM and incubated for 24 hours at 37°C under a 5% CO_2 atmosphere. The growth medium was replaced with 575 μl of pre-warmed bicarbonate-free DMEM, pH 7.4, and cells were incubated at 37°C for 1 hr before starting the assay. After baseline measurements, OCR was measured after sequentially adding to each well 75 μl of oligomycin, 75 μl of carbonyl cyanide-4-(trifluoromethoxy) phenylhydrazone (FCCP), 75 μl of rotenone and 75 μl of antimycin-A to reach working concentrations of (1 μM, 1 μM and 0.5 μM respectively). OCR values were normalized to cell number at the time of seeding. Furthermore, time dependent studies were normalized to basal respiration following a standard protocol (18).

2.7.e. Cell death: Cytotoxicity was determined using Cytotoxicity Detection Kit (Goode *et al*; Roche). In brief, media was collected at endpoints (in phenol red-free DMEM) to measure the percentage of released lactate dehydrogenase activity (LDH). To quantify total LDH, cells were lysed with lysis buffer (Cytotoxicity Detection Kit); 50 μl media or lysate was transferred with 50 μl of reaction mix in a 96-well plate and incubated at room temperature for 30 minutes in the dark. Absorbance was measured at 490 nm using SpectraMax M2e microplate reader (Molecular devices, CA), and cell death is presented as percent of released LDH of total LDH.

2.7. f. Lysosomal accumulation Assay: Cells were plated in 96-well plates and treated as previously described in section 2.2 and 2.3. At the end of the experiment, cells were incubated for 30 min with Lyso-ID™ Red dye (Enzo life sciences), a cell permeable fluorescent probe which localizes to acidic vesicles (endosomes, lysosomes, late autophagosomes). Fluorescence was measured using an excitation of 540 nm and an emission of 680 nm, while Hoechst dye (blue fluorescence) was determined with an excitation of 340 nm and an emission of 480 using a SpectraMax M2e (Molecular devices).

2.8. Isolation of Mitochondria-Enriched Fraction and Lysate Preparation

Cultured cells (3.75×10^6 cells in 10 cm dishes per condition) were scraped off in DMEM, washed once with cold phosphate-buffered saline (PBS) and re-suspended in mannitol–sucrose (MS) buffer, containing 210 mM mannitol, 70 mM sucrose, 5 mM MOPS (3-(N-morpholino) propane-sulfonic acid), 1 mM EDTA, and a protease inhibitor cocktail, pH 7.4. The cells were then disrupted by repeated aspiration through a 27½-gauge needle (20 times), while avoiding foaming. Heart tissues were sliced into small pieces using a scalpel and homogenized in MS buffer added with protease-inhibitor cocktail on ice using a tissue homogenizer (Biospec Products, Inc., OK). The homogenates were then spun at 800 g for 15 minutes at 4°C to extract the nuclear pellet. The resulting supernatants were aliquoted and used as total lysates. A second aliquot was centrifuged at 10,000 g for 40 minutes at 4°C. The pellets were surface-washed with MS buffer and extracted as mitochondria-rich fractions by re-suspending in MS buffer containing 0.1% Triton X-100 and protease inhibitor cocktail.

2.9. Western Blot Analysis

Protein concentrations were determined using the Bradford assay (Thermo Fisher Scientific) and then re-suspended in Laemmli buffer containing 2-mercaptoethanol, loaded on SDS–PAGE, and transferred on to nitrocellulose membrane, 0.45 μm (Bio-Rad), as described before (15). Membranes were probed with the indicated antibody and then visualized by ECL (0.225 mM p-coumaric acid; Sigma), 1.25 mM 3-aminophthalhydrazide (Luminol; Fluka) in 1 M Tris pH 8.5. Scanned images of the exposed X-ray film were analyzed with ImageJ to determine relative band intensity. Quantification was performed on samples from independent cultures for each condition.

2.10. Detection of S-nitrosylated Proteins in Total Heart Lysates

Detection of ROS-induced formation of S-nitrosylated proteins in total heart lysates was carried according to manufacturer's protocol (Pierce S-Nitrosylation Western blot kit, Thermo Scientific, MA). Briefly, all protein samples (adjusted to starting concentration of 2mg/ml to 100μl volume in HENS buffer) were first treated with a sulfhydryl-reactive compound, MMTS, that blocked all unmodified cysteines. Then, the remaining S-nitrosylated cysteins were reduced with sodium ascorbate (or not reduced, as a negative control to the experiment) and subsequently labeled with iodo-TMT reagent. Finally, the total lysate was run on Western blot, and the iodo-TMT labeled (i.e., S-nitrosylated) proteins were detected by an anti-TMT antibody (1:1000, Thermo Scientific). For quantification of S-nitrosylation level of each sample, it was normalized to total protein level as detected by

Ponceau-S staining of the sample. S-nitrosylation bands were not detected in the non-reduced samples.

2.11. Electron Microscopy

The hearts from the BALB/c mice were carefully flushed using saline and dissected for further for fixation. Once blood was removed from the cardiac chambers, tissue was fixed in 2.5% glutaraldehyde in 0.1 mol/l cacodylate buffer, pH-7.4. The fixed material was sectioned at the Stanford Electron Microscopy Facility. Sections were taken between 75 and 80 nm, picked up on formvar/carbon-coated 75 mesh Ni grids and stained for 20 s in 1:1 saturated uracetate (≈7.7%) in acetone followed by staining in 0.2% lead citrate for 3–4 minutes for contrast. For each sample, two tissue blocks (volume of 5 mm^3) were cut to obtain an average of 20 grids. Tissue samples were observed in a JEOL 1230 transmission electron microscope at 80 kV, and photographs were taken using a Gatan Multiscan 791 digital camera.

Cardiac muscle architecture was examined based on intersarcomeric area, defined by the space intermingled between two sarcomers as well as density of mitochondria in the muscle, defined by the number of mitochondria per surface unit as described earlier. Mitochondria were defined as altered according to criteria being validated by previous morphological studies (i) significantly decreased electron density of the matrix (dilution, vacuolization, cavitation); (ii) fragmented and ballooned cristae (intracristal swelling); (iii) partial or complete separation of the outer and inner membranes; (iv) mitochondrial swelling (23). Quantitative analysis of mitochondrial damage was performed independently by two investigators, who reviewed each enlarged electron microscopy image for the presence of structurally abnormal mitochondria.

2.12. Extraction and Quantification of Mitochondrial DNA Content

2.12.a Total DNA extraction from mouse hearts—Snap-frozen mouse heart slices from −80°C were lysed in Buffer ATL and proteinase K at 56°C overnight on a thermomixer using TissueLyser (QIAamp DNA Investigator Kit, Qiagen). Total DNA (genomic + mitochondrial) was extracted from the tissue lysates using Quick-DNA Miniprep Kit (Zymo Research) according to manufacturer's instruction. Before proceeding to qPCR, the DNA templates were subjected to shearing and reducing viscosity by passing them through 21G needles for >2 minutes, as described previously, (22) to avoid dilution bias. The template concentration was determined using NanoDrop and adjusted to 10 ng/μl. To avoid errors arising from repeated freeze thaw cycles, DNA samples were kept at 4°C for the duration of study.

2.12.b Quantification of mitochondrial DNA content—Mitochondrial DNA (mtDNA) content was assessed by absolute quantification of DNA copy numbers using real time PCR. Since duplication of mtDNA in nuclear DNA (known as nuclear mitochondrial insertion sequences or NumtS) affects accurate quantification of mtDNA copy numbers, primers designed against unique regions of mtDNA that do not house NumtS (21) were used for mtDNA amplification (mMitoF1, mMitoR1). To measure nuclear DNA copy number, primers against single copy nuclear gene, beta-2 microglobulin (B2M) were used (21).

Sequences of the primers can be found on supplemental table and detailed protocol is as described in (21). Briefly, respective mtDNA and nuclear DNA products (125 bp mtDNA product and 177 bp nuclear DNA product) were first amplified from mouse heart genomic DNA samples (10 ng/μl) using the following protocol: pre-incubation at 95°C for 5 minutes (1 cycle); denaturation at 95°C for 30 seconds, annealing at 52°C for 30 sec, extension at 72°C for 45 sec (repeat steps for 40 cycles), and final extension at 72°C for 5 minutes. PCR products were gel purified and used to prepare serial dilution standards for both amplicons at a range of 10^1–10^9 copies/μl to allow absolute quantification. MtDNA and nuclear DNA copy numbers per cell were then determined from template DNA samples (10 ng/μl) by carrying out qPCR in a total volume of 20 μl, containing 10 μl of iTaq Universal SYBR Green Supermix (Biorad), 0.1 μl of 100 μM forward primer, 0.1 μl of 100 μM reverse primer, 8.8 μl of Ultrapure water and 1 μl template DNA. The reactions were performed in Biorad CFX Connect qPCR instrument using the following protocol: pre-incubation at 95°C for 5 minutes (1 cycle); denaturation at 95°C for 10 s, annealing and extension at 60°C for 30 s (repeat denaturation and extension steps for 40 cycles). The thermal profile for melt curve analysis began with melting at 95 °C for 1 minute, at 65°C for 1 minute and then an incubation of 5 seconds at 65°C with a gradual increase in temperature to 95°C at the rate of 0.5°C/5 seconds, during which time changes in fluorescence were monitored. A last cooling step was included at 40°C for 30 seconds. The specificity of the primers (one PCR product amplified) was confirmed as a single melt peak and single band when electrophoresed on 2% agarose gel for both amplicons. qPCR efficiencies calculated from the slope of the standard curves were 86% with co-efficiency of reaction R^2 = 0.98–0.99. Mitochondrial content was calculated as a ratio of mtDNA copy number/Nuclear DNA copy number X 2 (21).

2.13 siRNA transfection

Rat-specific Fis1-siRNAs were obtained from Qiagen (Flexitube siRNA; Cat#SI01544438 and SI01544445) and transfected into H9C2 cardiomyocytes (initially seeded at 30–40% confluency in 6-well plates) at 50, 30 or 10 nM concentrations to optimize sufficient Fis1 knockdown by the siRNA.

Once optimal concentration of Fis1-siRNA was selected, H9C2 cells were seeded at a density of 3000 cells/well in 96-well plates in 10% FBS media. Next day, the cells were transfected with 50 nM of Fis1-siRNA, using 0.3 μl/well Lipofectamine2000 (Thermo Fisher Scientific) in serum-free media. Media were changed to 10% FBS media 5–6 hours after siRNA transfection. On the next day, cells were treated with or without 0.5 ug/ml LPS from *E.coli* 0111:B4 (Sigma, lot #: 014M4019V) in 0.5% FBS media and following addtional 24 hours, cells were processed for mitochondrial health assays (TMRM & MitoSox), as described above.

2.14. Plasmid vector modification and transfection

H9C2 cells were seeded at a density of 50,000 cells/well in 12-well plates in 10% FBS media. Next day, they were transfected with 1.6 μg of mCh-Drp1-WT or mCh-Drp1-S616E plasmids, using 4 μl Lipofectamine2000 (Thermo Fisher Scientific) volume/well in serum-

free media. Media were changed to 10% FBS media 5–6 hours after siRNA transfection and 48 hours later, cells were processed for cytotoxicity assay.

2.15. Statistics

Data are expressed as means ± SEM. Statistical analysis was assessed by Student's T-test for studies that had 2 groups and ANOVA for studies with 3 or greater groups. Significance in cell culture experiments was analyzed with the Tukey's *post hoc* test. The standard Mantel–Cox log-rank test was used to assess survival. All statistical analyses were conducted on biological replicates for each experiment using GraphPad Prism software. For the cell culture studies, we performed at least three independent experiments, in duplicates. An observer who was blind to the experimental groups conducted all the tissue data analysis. The nominal p value of <0.05 was used as statistically significant threshold, and *, **, ***, ****, correspond to $p < 0.05$, < 0.01, < 0.001, and 0.0001, respectively.

3. Results

3.1. Sepsis-induced mitochondrial fission is associated with mitochondrial dysfunction and increased mitochondrial oxidative stress.

When evaluating changes in mitochondrial morphology, we found excessive mitochondrial fragmentation, as evidenced by small and more circular mitochondrial staining patterns (Figure 1A), as early as 12–24 hours following LPS treatment in the H9C2 cell line model of sepsis (Supplemental Figure 1). This change in mitochondrial morphology after LPS coincided with a significant drop in mitochondrial membrane potential, observed as early as 6 h post LPS (TMRM control = 2.7± 0.2 *vs.* 6 h LPS=1.9± 0.2, p=0.04) (Figure 1B) as well as bioenergetic failure, as evidenced by a significant drop in maximal respiration (MAX; control = 728 ± 160 pmol/min *vs.* LPS 6 h =587 ± 161 pmol/min, p=0.03) and spare respiratory capacity (SRC; control = 445 ± 107 pmol/min *vs.* 12 h LPS=299 ± 55 pmol/min, p<0.001) using Seahorse oximetry (Figure 1E). We also observed a 50% increase in mitochondrial-specific oxidative stress at 24h which doubled from baseline by 48 h following LPS treatment (MitoSOX, p<0.001) (Figure 1C), signifying a link between mitochondrial fragmentation and ROS production in sepsis.

3.2. Drp1 activation and mitochondrial association is essential for sepsis-induced mitochondrial fragmentation in the H9C2 cardiomyocyte model of sepsis.

To understand changes in activation and localization patterns of Drp1 in sepsis, we first evaluated changes in phosphorylation states of Drp1 following LPS treatment in H9C2 cells. Since previous studies have shown that Drp1 phosphorylation at serine 616 precedes mitochondrial localization of Drp1 and subsequent mitochondrial damage, we evaluated Drp1 phosphorylation at early time points. Accordingly, phosphorylation of Drp1 at Ser616, which correlates with Drp1 activation and promotes fission (26), increased by 3-fold as early as 1–2 h. following LPS (Figure 2A). There was also a dramatic 11-fold increase in mitochondrial Drp1 at 4hrs. following LPS treatment (p<0.001; Figure 2B). Drp1 activation and localization was followed by a six-fold decrease in mitochondrial mass in cells treated with LPS, as measured by the reduction in total levels of VDAC and TIM22, markers of outer and inner mitochondrial membranes, respectively (p<0.001; Figure 2C). Furthermore,

LPS-induced alteration in mitochondrial function and dynamics was also associated with approximately 60% increase in lysosomal accumulation and 30% increase in cell death by 48hrs (Figure 2D, E). Similarly, expression of phosphomimetic Drp1 mutant (Drp1-S616E) in H9c2 cardiomyocytes resulted in increased cell death, as represented by increased LDH release within 48hrs (Supplemental Figure 2C). These findings suggest that LPS-mediated activation of Drp1 is associated with marked mitochondrial fragmentation, leading to a decrease in mitochondrial content, lysosomal activation and eventual cell death.

3.3 Inhibition of Drp1/Fis1 interaction using P110 attenuates disruption of cellular respiration and limits cell death in vitro.

Since Drp1 recruitment from the cytosol to the outer mitochondrial membrane is a hallmark of fission and since Drp1/Fis1 interaction has been linked with pathologic mitochondrial fragmentation in neurodegenerative diseases and ischemic heart disease (19,20,25,36), we hypothesized that blocking Drp1/Fis1 interaction, using P110 (a peptide designed to inhibit Drp1/Fis1 interaction (16)), would abrogate pathological fission in H9C2 cardiomyocytes. As expected, P110 treatemt reduced mitochondrial Drp1 localization (Figure 3A), greatly improved cellular respiration (increased maximum respiration as well as SRC) (Figure 3B), blocked LPS-induced loss of mitochondrial membrane potential, and significantly reduced mitochondrial ROS production (Figure 3C & D).

These findings were further validated by transiently repressing Fis1 expression in the H9C2 cardiomyocyte model of sepsis. Results from this experiment demonstrated decreased mitochondrial oxidative stress and improved mitochondrial membrane potential by Fis1 repression in this LPS model (Supplemental Figure 2), highlighting the importance of Fis1/Drp1-dependnet pathway in sepsis induced mitochondrial dysfunction.

As previously mentioned, a certain baseline level of mitochondrial fission is necessary for physiological cellular function and mitochondrial quality control. This is thought to be mediated through alternate mitochondrial adaptors including mitochondrial fission factor Mff (19,23). To determine the role of Drp/Mff interaction, we used P259, a peptide we developed to selectively interfere with the Drp1/Mff interaction (13). Whereas P110 rescued mitochondrial membrane potential, ATP production and decreased lysosomal accumulation (Figure 4B, C), peptide P259 caused an increase in both mitochondrial and total oxidative stress ($p < 0.001$; Figure 4A), as well as an increase in cell death when compared to cells treated with LPS alone ($p < 0.001$; Figure 4C), similar to its deleterious effects in models of Huntington's disease (13).

3.4: Inhibition of Drp1/Fis1 interaction using P110 is protective in the LPS mouse model of sepsis

Next, we utilized an established LPS model of sepsis (28) in 5–7-week old female BALB/c mice, to evaluate the role of Drp1-Fis1 interaction in sepsis-mediated cardiomyopathy. P110 treatment reduced illness severity, evidenced by significantly reduced weight loss, normalization of body temperature and an ~50% decrease in cumulative mouse sepsis score ($p< 0.001$). Importantly, P110 treatment reduced mortality by 30% ($p=0.008$) at 48 hours (which was sustained through 94 hours) relative to LPS treatment alone (Figure 5A).

When evaluating cardiac function, LPS treatment resulted in a significant decrease in cardiac function, as measured by fractional shortening at 6 hrs. as well as velocity time integral (VTI) across the left ventricular outflow tract 12 and 24 hrs. following LPS treatment. This decrease was prevented by treatment with P110 (delta VTI at 24hrs.; control = 0.28± 2.22 *vs.* LPS= −8.87±2.18 *vs.* LPS + P110= 3.31.3±2.55, P=0.004) (Figure 5B).

To examine the influence of Drp1/Fis1 inhibition on septic cardiomyopathy at a cellular level, we utilized electron microscopy to evaluate cardiac mitochondrial morphology from mice in the three treatment groups (control, LPS, LPS +P110). Results from this experiment demonstrated that LPS-treated mice had extensive mitochondrial swelling, fragmentation, and myofibril structural disarray within 24 hours (Figures 6A–E) when compared to controls. This was accompanied by a significant increase in cardiac oxidative stress, as represented by a 5-fold increase in oxidative post-translational modification (s-nitrosylation) (Figure 6F) and a decrease in mitochondrial content, represented by a 2.5-fold decrease in mitochondrial DNA content (Figure 6G). Interestingly, inhibition of Drp1/Fis1 interaction with P110 in the septic mice, significantly reduced cardiac mitochondrial fragmentation (increased aspect ratio, form factor and cross section area) (Figures 6A–E), and cardiac oxidative stress (S-Nitrosylation) (Figure 6F) and prevented the decrease in mitochondrial content (Figure 6G).

4. Discussion

Although the significance of SIMD is well established as a risk factor for mortality in patients with sepsis, the mechanisms underlying this pathology remain unclear. Notable headway was made when Parrillo and colleagues theorized the presence of an, as yet unidentified, circulating myocardial depressant factor (MDF) to be a major contributor of SIMD (4) (29). A recent focus on “cytopathic hypoxia,”, disturbance of cellular bioenergetics in sepsis, identified the influence of mitochondrial oxidative stress on multi-organ system failure and mortality (11, 30). Here, we demonstrate a critical role for mitochondrial fragmentation in the development of cardiac oxidative damage and cardiac dysfunction in sepsis. Excessive mitochondrial fragmentation, mediated through the Drp1/Fis1 interaction, has been shown to induce oxidative stress in a variety of disease models, including ischemia/reperfusion and neurodegenerative diseases (12–15,19,20). We show that selective inhibition of Drp1/Fis1 interaction, using P110, reduces pathological mitochondrial fission, rescues cellular respiration and improves ATP production in a cardiac cell line model of sepsis. Similarly, treatment with P110 3 hrs after LPS injection prevented cardiac dysfunction, reduced illness severity and improved survival in mice subjected to LPS-induced sepsis. Peptide P110 was rationally designed based on sequence homology search between Drp1 and Fis1. It selectively inhibits Drp1/Fis1 interaction and has no effect on Drp1 interaction with any other mitochondrial fission adaptors (Mff, Mid49, Mid 51) (11,14–16). The mechanistic efficacy of this peptide has been demonstrated in previous studies where P110 selectively inhibits excessive mitochondrial fission with no significant effect on baseline (physiological) mitochondrial turnover (19,15). Importantly, even a five-month sustained treatment with P110 (at 3mg/kg/day) caused no discernable side effects; rather, it may slow down age-related motor loss in neurodegenerative models (15,16,20).

Whereas excessive mitochondrial fission is detrimental for cellular function, baseline mitochondrial fission is necessary for effective mitochondrial quality control. Indeed, inhibition of baseline physiological fission with P259, a peptide that we designed to selectively inhibit Drp1/Mff interaction (13), led to worsening of LPS-induced oxidative stress and mitochondrial failure in H9C2 cells, similar to its deleterious effects in a model of Huntington's disease (13). These findings suggest that sepsis-mediated pathological mitochondrial fragmentation is specific to Drp1/Fis1 interaction.

In the LPS-mouse model of sepsis, cardiac dysfunction, represented by a decrease in VTI, was prevented by peptide P110 treatment. Although volumetric assessment of left ventricular function (EF, FS) and subjective assessment of right ventricular function are often used as a non-invasive surrogate of cardiac function in critical illness, these metrics are significantly limited by changes in loading conditions and altered wall motion associated with sepsis (31,32). In contrast, left ventricular outflow tract velocity time integral (LVOT-VTI), a Doppler-derived measure of stroke volume, can be easily obtained, is independent of ventricular geometry and wall motion abnormalities and has been shown to be a more sensitive metric of cardiac function (33).

4. Limitations:

Although our study suggests that Drp1/Fis1-mediated mitochondrial fission is an important mechanism of cardiac dysfunction in the setting of sepsis, there are several limitations that need to be considered. One limitation is the use of an immortalized cell line for the sepsis experiments. H9C2 cells are myoblasts derived from rat ventricles with a long history of use in cardiovascular research due to their similarities in metabolism to primary cardiomyocytes (34). Therefore, additional studies are needed to further validate our findings in human cardiomyocytes.

Another limitation is the use of LPS in the model of sepsis. LPS use in murine model of sepsis enables consistency in illness severity and mortality rate. Despite being well established model of sepsis over the past 40 years, some have challenged the ability of LPS models to fully recapitulate the clinical sepsis phenotype (35). In particular, the fact that this model is founded on a primary systemic inflammatory challenge without an infectious focus is a discordance from the characteristics of human sepsis. Thus, future studies utilizing other sepsis models, including cecal ligation and puncture or klebsiella pneumonia, are imperative in further validating the role of Drp1/Fis1-mediated mitochondrial dysfunction in sepsis. Finally, future studies are needed to determine the optimal dosing and treatment intervals for cardio-protection in other sepsis models.

In summary, we have identified the Drp1/Fis1 interaction as the mechanism responsible for marked pathologic alterations in cardiac mitochondrial function and morpholgy, and as an important contributor to SIMD. Evaluation of the therapeutic potential for fission inhibitors, like P110, will require further large animal and clinical studies, however, we have set the stage for potential new therapeutic strategies to reduce the substantial risk of cardiac failure and death in patients with sepsis.

Supplementary Material

Refer to Web version on PubMed Central for supplementary material.

Acknowledgements:

The authors thank John Perrino at Stanford University for technical support with EM and Professor Noriyuki Matsuda's laboratory at the Tokyo Metropolitan Institute of Medical Sciences for providing plasmid pSu9-GFP for life microscopy.

Funding: This work was supported in part by Stanford Maternal Child Health Research Institute Pilot Early Career award and 5K12HD047349 to BH and byHL52141 to DM-R.

References:

1). Hartman ME, Linde-Zwirble WT, Angus DC, & Watson RS (2013). Trends in the epidemiology of pediatric severe sepsis. Pediatric Critical Care Medicine, 14(7), 686–693. [PubMed: 23897242]

2). Rubens M, Saxena A, Ramamoorthy V, Das S, Khera R, Hong J, … & Gidel L (2018). Increasing Sepsis Rates in the United States: Results from National Inpatient Sample, 2005 to 2014. Journal of intensive care medicine, 0885066618794136.

3). Weiss SL, Balamuth F, Hensley J, Fitzgerald JC, Bush J, Nadkarni VM, … & Muszynski J (2017). The epidemiology of hospital death following pediatric severe sepsis: when, why, and how children with sepsis die. Pediatric Critical Care Medicine, 18(9), 823–830 [PubMed: 28549024]

4). Court O, Kumar A, Parrillo JE. Clinical review: Myocardial depression in sepsis and septic shock. Crit Care. 2002;6(6):500–508. [PubMed: 12493071]

5). Antonucci E, Fiaccadori E, Donadello K, Taccone FS, Franchi F, Scolletta S. Myocardial depression in sepsis: from pathogenesis to clinical manifestations and treatment. J Crit Care 2014;29(4):500–511.. [PubMed: 24794044]

6). Arulkumaran N, Deutschman CS, Pinsky MR, Zuckerbraun B, Schumacker PT, Gomez H, … & Kellum JA (2016). Mitochondrial function in sepsis. Shock (Augusta, Ga.), 45(3), 271.

7). Spapen HD, Jacobs R, & Honoré PM (2017). Sepsis-induced multi-organ dysfunction syndrome—a mechanistic approach. Journal of Emergency and Critical Care Medicine, 1(10).

8). Wesche-Soldato DE, Swan RZ, Chung CS, & Ayala A (2007). The apoptotic pathway as a therapeutic target in sepsis. Current drug targets, 8(4), 493–500. [PubMed: 17430119]

9). Turrel-Davin F, Guignant C, Lepape A, Mougin B, Monneret G, & Venet F (2010). Upregulation of the pro-apoptotic genes BID and FAS in septic shock patients. Critical Care, 14(4), R133. [PubMed: 20626850]

10). Weiss SL, Balamuth F, Hensley J, et al. The Epidemiology of Hospital Death Following Pediatric Severe Sepsis: When, Why, and How Children With Sepsis Die. Pediatr Crit Care Med 2017;18(9):823–830. [PubMed: 28549024]

11). S Weiss SL, Selak MA, Tuluc F, Villarroel JP, Nadkarni VM, Deutschman CS, & Becker LB (2015). Mitochondrial dysfunction in peripheral blood mononuclear cells in pediatric septic shock. Pediatric critical care medicine: a journal of the Society of Critical Care Medicine and the World Federation of Pediatric Intensive and Critical Care Societies, 16(1), e4.

12). Kornfeld OS, Hwang S, Disatnik MH, Chen CH, Qvit N, & Mochly-Rosen D (2015). Mitochondrial reactive oxygen species at the heart of the matter: new therapeutic approaches for cardiovascular diseases. Circulation Research, 116(11), 1783–1799. [PubMed: 25999419]

13). Kornfeld OS, Qvit N, Haileselassie B, Shamloo M, Bernardi P, & Mochly-Rosen D (2018). Interaction of mitochondrial fission factor with dynamin related protein 1 governs physiological mitochondrial function in vivo. Scientific reports, 8(1), 14034. [PubMed: 30232469]

14). Joshi AU, Saw NL, Vogel H, Cunnigham AD, Shamloo M, & Mochly-Rosen D (2018). Inhibition of Drp1/Fis1 interaction slows progression of amyotrophic lateral sclerosis. EMBO molecular medicine, e8166. [PubMed: 29335339]

15). Joshi AU, Saw NL, Shamloo M, & Mochly-Rosen D (2018). Drp1/Fis1 interaction mediates mitochondrial dysfunction, bioenergetic failure and cognitive decline in Alzheimer's disease. Oncotarget, 9(5), 6128. [PubMed: 29464060]

16). Qi X, Qvit N, Su YC, & Mochly-Rosen D (2013). A novel Drp1 inhibitor diminishes aberrant mitochondrial fission and neurotoxicity. J Cell Sci, 126(3), 789–802. [PubMed: 23239023]

17). Shrum B, Anantha RV, Xu SX, Donnelly M, Haeryfar SM, McCormick JK, & Mele T (2014). A robust scoring system to evaluate sepsis severity in an animal model. BMC research notes, 7(1), 233. [PubMed: 24725742]

18). de Moura MB, & Van Houten B (2014). Bioenergetic analysis of intact mammalian cells using the Seahorse XF24 Extracellular Flux analyzer and a luciferase ATP assay In Molecular Toxicology Protocols (pp. 589–602). Humana Press, Totowa, NJ.

19). Joshi AU, & Mochly-Rosen D (2018). Mortal engines: Mitochondrial bioenergetics and dysfunction in neurodegenerative diseases. Pharmacological research

20). Guo X, Disatnik MH, Monbureau M, Shamloo M, Mochly-Rosen D, Qi X (2013) Inhibition of mitochondrial fragmentation diminishes Huntington's disease-associated neurodegeneration. J Clin Investigation 123: 5371–5388

21). Malik Afshan N., Czajka Anna, and Cunningham Phil. "Accurate quantification of mouse mitochondrial DNA without co-amplification of nuclear mitochondrial insertion sequences." Mitochondrion 29 (2016): 59–64. [PubMed: 27181048]

22). Ajaz S, Czajka A, & Malik A (2015). Accurate measurement of circulating mitochondrial DNA content from human blood samples using real-time quantitative PCR In Mitochondrial Medicine (pp. 117–131). Humana Press, New York, NY.

23). Dagda RK, Cherra SJ III, Kulich SM, Tandon A, Park D, Chu CT (2009) Loss of PINK1 function promotes mitophagy through effects on oxidative stress and mitochondrial fission. J Biol Chem 284: 13843–13855 [PubMed: 19279012]

24). Wiemerslage L, Lee D (2016) Quantification of mitochondrial morphology in neurites of dopaminergic neurons using multiple parameters. J Neurosci Methods 262: 56–65 [PubMed: 26777473]

25). Qi X, Disatnik MH, Shen N, Sobel RA, & Mochly-Rosen D (2011). Aberrant mitochondrial fission in neurons induced by protein kinase Cδ under oxidative stress conditions in vivo. Molecular biology of the cell, 22(2), 256–265. [PubMed: 21119009]

26). Cho B, Choi SY, Cho HM, Kim HJ, & Sun W (2013). Physiological and pathological significance of dynamin-related protein 1 (drp1)-dependent mitochondrial fission in the nervous system. Experimental neurobiology, 22(3), 149–157. [PubMed: 24167410]

27). Osellame LD, Singh AP, Stroud DA, Palmer CS, Stojanovski D, Ramachandran R, & Ryan MT (2016). Cooperative and independent roles of the Drp1 adaptors Mff, MiD49 and MiD51 in mitochondrial fission. J Cell Sci, 129(11), 2170–2181. [PubMed: 27076521]

28). Remick DG, Newcomb DE, Bolgos GL, & Call DR (2000). Comparison of the mortality and inflammatory response of two models of sepsis: lipopolysaccharide vs. cecal ligation and puncture. Shock (Augusta, Ga.), 13(2), 110–116.

29). Parrillo JE, Burch C, Shelhamer JH, Parker MM, Natanson C, & Schuette W (1985). A circulating myocardial depressant substance in humans with septic shock. Septic shock patients with a reduced ejection fraction have a circulating factor that depresses in vitro myocardial cell performance. The Journal of clinical investigation, 76(4), 1539–1553. [PubMed: 4056039]

30). Singer M (2014). The role of mitochondrial dysfunction in sepsis-induced multi-organ failure. Virulence, 5(1), 66–72. [PubMed: 24185508]

31). Haileselassie B, Su E, Pozios I, Fiskum T, Thompson R, Abraham T. Strain Echocardiography Parameters Correlate With Disease Severity in Children and Infants With Sepsis. Pediatr Crit Care Med 2016;17(5):383–390. [PubMed: 26963758]

32). Basu S, Frank LH, Fenton KE, Sable CA, Levy RJ, Berger JT. Two-dimensional speckle tracking imaging detects impaired myocardial performance in children with septic shock, not recognized by conventional echocardiography. Pediatr Crit Care Med 2012;13(3):259–264. [PubMed: 21760563]

33). Navaratnam M, Punn R, Ramamoorthy C, & Tacy TA (2017). LVOT-VTI is a Useful Indicator of Low Ventricular Function in Young Patients. Pediatric cardiology, 38(6), 1148–1154. [PubMed: 28534242]

34). Kuznetsov AV, Javadov S, Sickinger S, Frotschnig S, & Grimm M (2015). H9C2 and HL-1 cells demonstrate distinct features of energy metabolism, mitochondrial function and sensitivity to hypoxia-reoxygenation. Biochimica et Biophysica Acta (BBA)-Molecular Cell Research, 1853(2), 276–284. [PubMed: 25450968]

35). Rittirsch D, Hoesel LM, & Ward PA (2007). The disconnect between animal models of sepsis and human sepsis. Journal of leukocyte biology, 81(1), 137–143. [PubMed: 17020929]

36). Disatnik MH, Ferreira JC, Campos JC, Gomes KS, Dourado PM, Qi X, & Mochly-Rosen D (2013). Acute inhibition of excessive mitochondrial fission after myocardial infarction prevents long-term cardiac dysfunction. Journal of the American Heart Association, 2(5), e000461. [PubMed: 24103571]

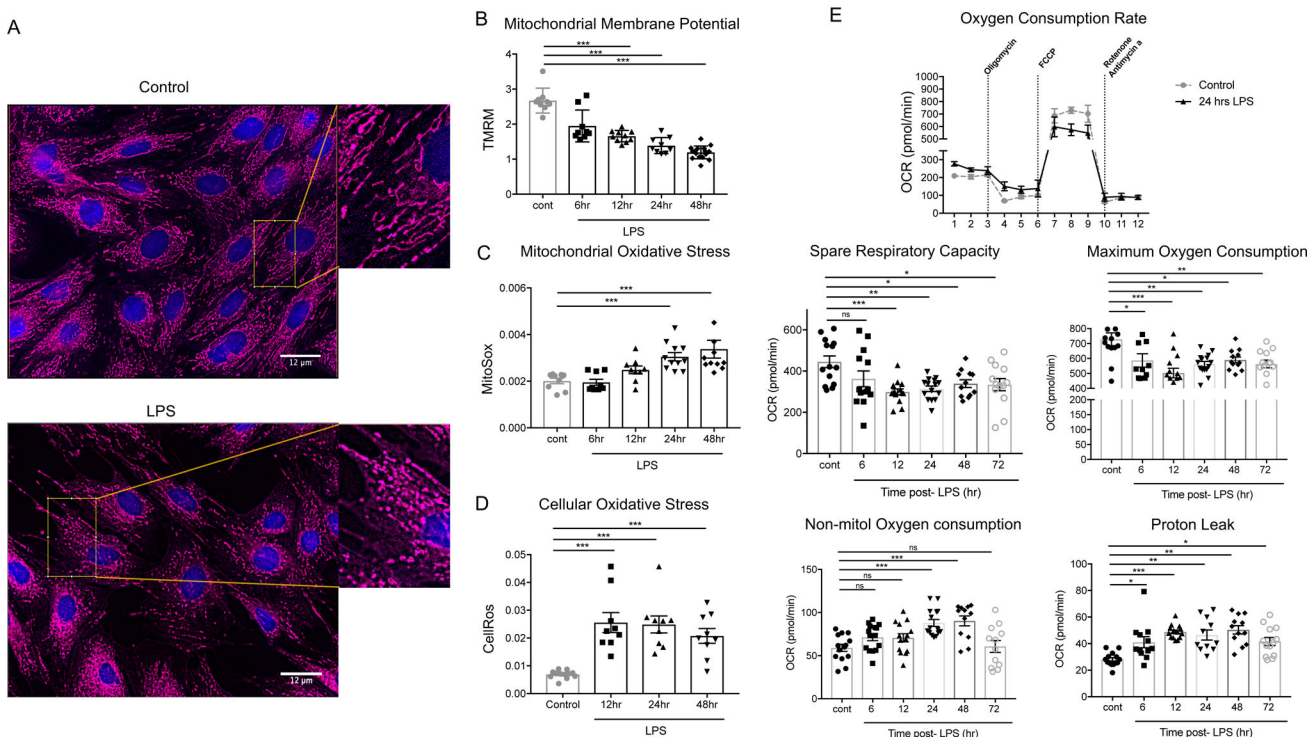

Figure 1:

Sepsis-induced mitochondrial fission is associated with mitochondrial dysfunction and increased mitochondrial oxidative stress. (A) Immunofluorescent microscopy co-stained with Mitotracker (purple) and Hoechst (blue) demonstrating mitochondrial fragmentation in H9C2 cardiomyocytes following 12 hrs. of LPS treatment. Mitochondrial fragmentation associated with mitochondrial dysfunction represented by: 1) decreased tetramethylrhodamine methyl ester (TMRM™) fluorescence (n=3 biological replicates). (B) as a surrogate for decreased membrane potential, 2) increased mitochondrial-specific ROS production (MitoSox™) (n=3 biological replicates). (C) and total cell ROS production (CellRos™). (D) (n=3 biological replicates) and 3) decreased cellular respiration, measured by changes in oxygen consumption rate on seahorse XF-24e at different time points following LPS treatment (n=5 biological replicates) (E).

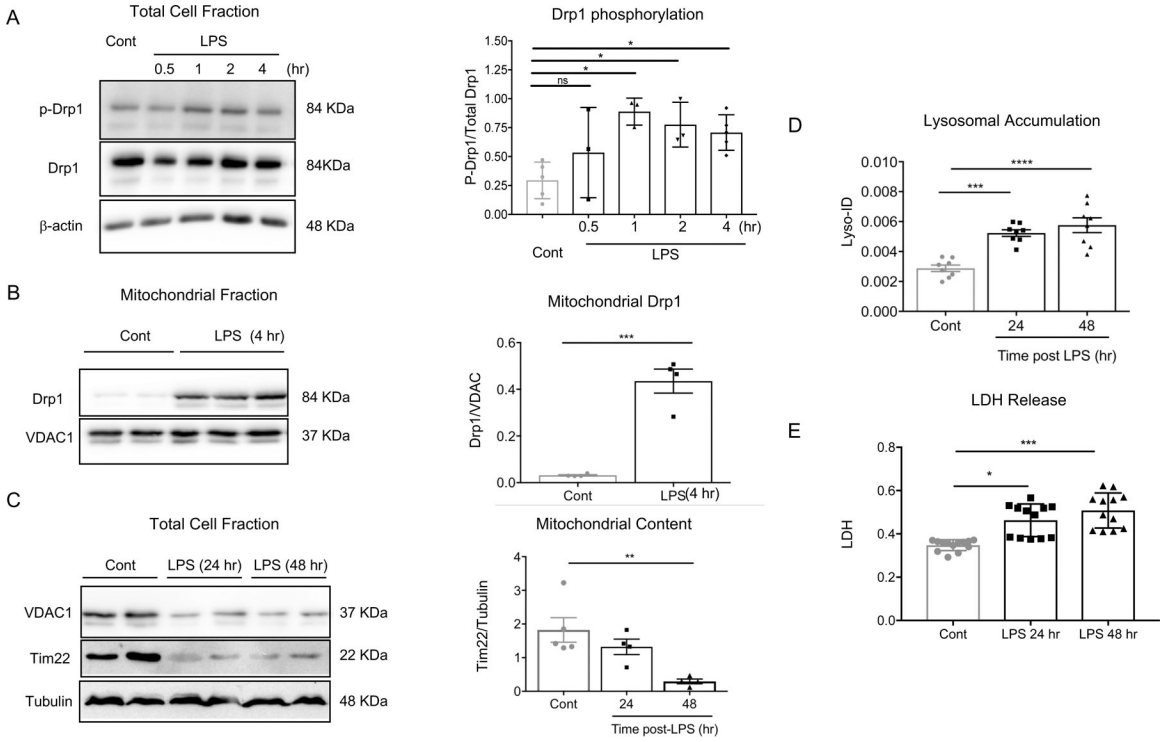

Figure 2:

(A) Western blot showing Drp1 phosphorylation levels in total lysate by immunoblotting using anti-phosporylated-S616-Drp1 antibodies at different time points following LPS treatment (n=3 biological replicates). (B) Western blot demonstrating Drp1 levels in mitochondrial-enriched fractions 4 hrs after LPS treatment as compared to control treatment (n=4 biological replicates). VDAC was used as a loading control and protein levels were quantified and represented as a ratio. (C) Mitochondrial content was evaluated using western blot analyses. VDAC and Tim22 were used as markers of outer and inner mitochondrial membrane and were normalized to tubulin (n=4 biological replicates). (D) Lysosomal accumulation quantified by fluorophore (Lyso-ID™) quantification normalized to Hoechst (n=4 biological replicates). (E) LDH release in the cell supernatant was utilized as a surrogate for cell death and quantified using Cytotoxicity Detection Kit (n=4 biological replicates).

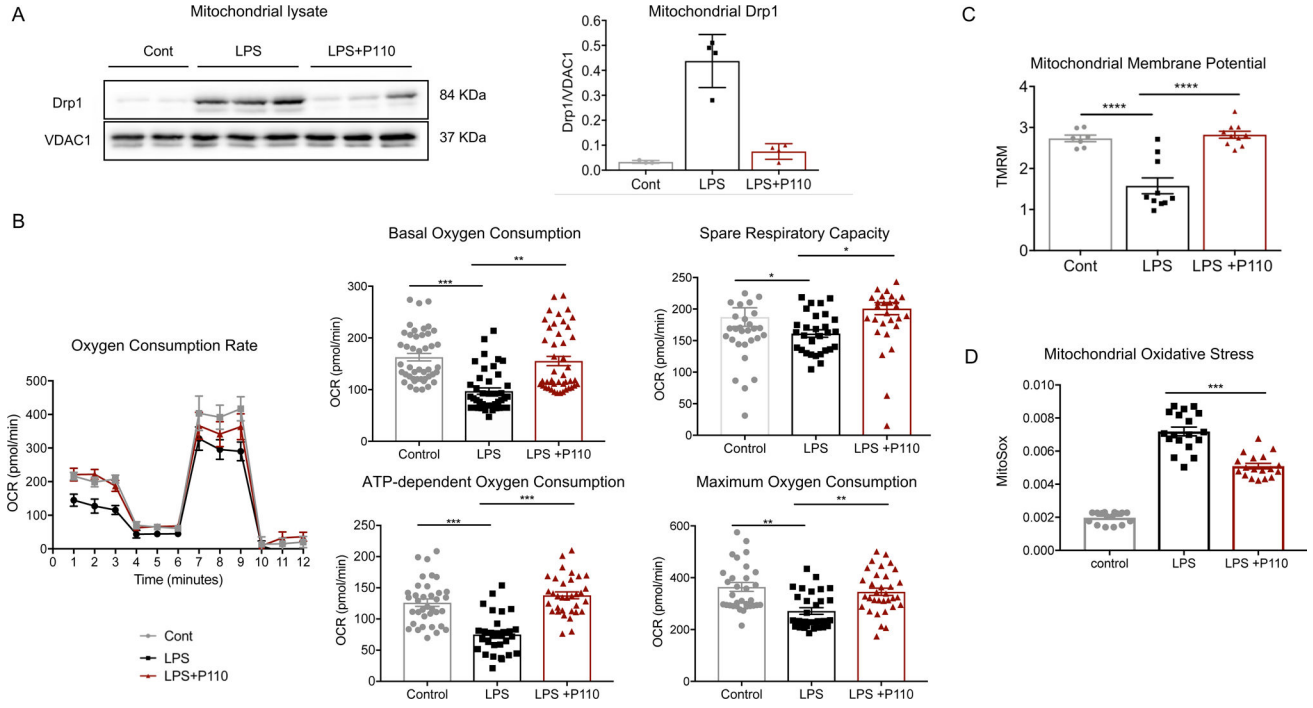

Figure 3:

(A) Western blot analysis demonstrating Drp1 levels in mitochondrial-enriched fractions in 3 conditions (control, LPS treated, LPS + P110 treated) after 24 hrs. (n=3 biological replicates). VDAC was used as a loading control and protein levels were quantified and represented as a ratio. (B) Cellular respiration measured by changes in oxygen consumption rate on seahorse XF-24e in control, LPS treatment and LPS+P110 treatment (n=6 biological replicates). Quantification for basal oxygen consumption, maximum oxygen consumption, spare respiratory capacity, ATP-dependent oxygen consumption presented in pmol/min. (C) Tetramethylrhodamine methyl ester (TMRM™) fluorescence utilized as a surrogate for mitochondrial membrane potential across the three groups. Quantification was normalized to Hoechst (n=3 biological replicates). (D) Increased mitochondrial-specific oxidative stress quantified by fluorescence assay (MitoSox™) and quantification normalized to Hoechst(n=4 biological replicates).

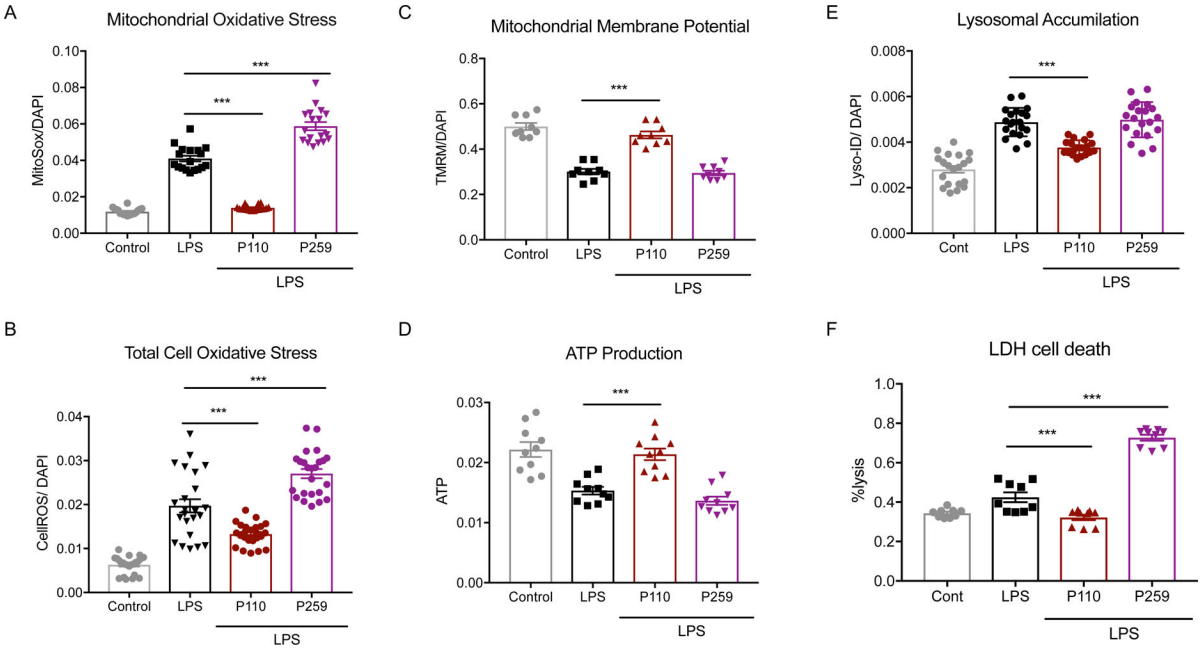

Figure 4:

Evaluation of mitochondrial function, oxidative stress, lysosomal accumulation and cell death in H9C2 cardiomyocytes stratified to 4 different conditions (control, LPS treatment, LPS along with P110 treatment, LPS along with P259 treatment). (A) Mitochondrial-specific ROS (MitoSox™) (n=4 biological replicates). and (B) total cell ROS (CellRos™) (n=4 biological replicates) were quantified and normalized to Hoechst. (C) Tetramethylrhodamine methyl ester (TMRM™) fluorescence utilized as a surrogate for mitochondrial membrane potential across the 4 groups (n=3 biological replicates). (D) ATP production was quantified by ATP colorimetric/fluorometric assay kit (Biovision, Milpitas, CA) (n=3 biological replicates). (E) Lysosomal accumulation was quantified by fluorophore (Lyso-ID™) quantification normalized to Hoechst (n=5 biological replicates). (F) LDH release in the cell supernatant was utilized as a surrogate for cell death and quantified using Cytotoxicity Detection Kit (n=3 biological replicates).

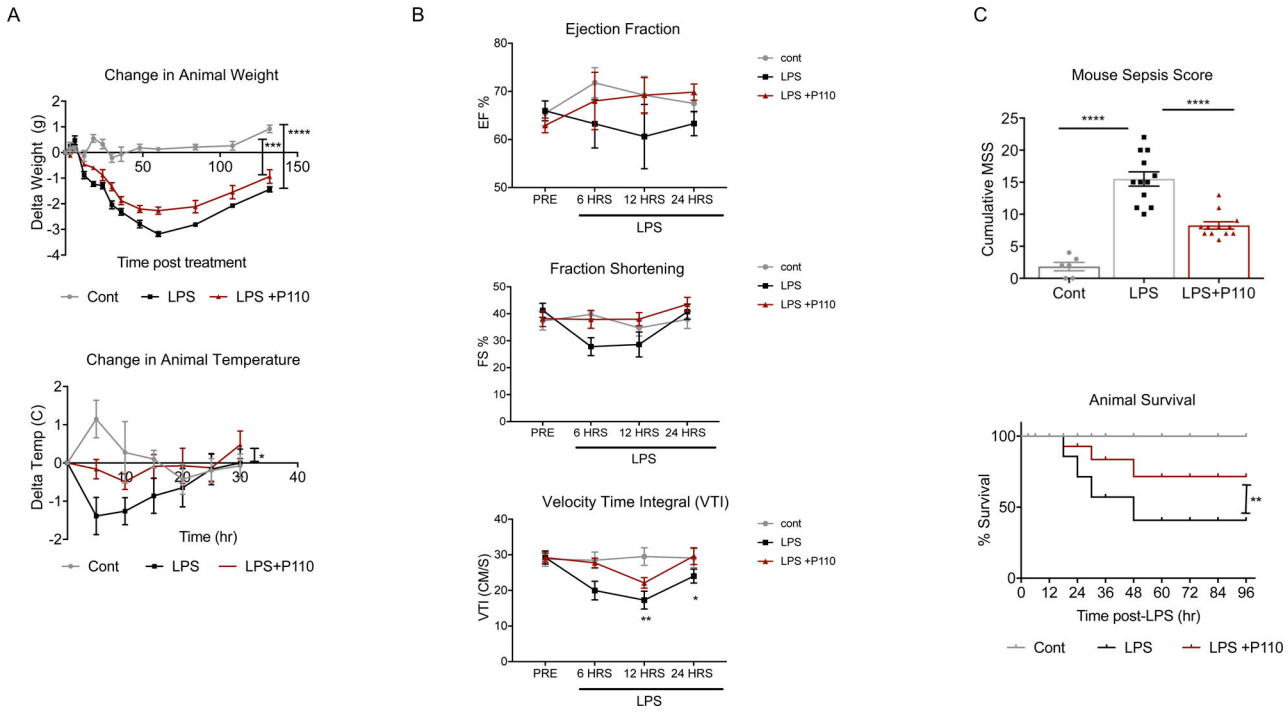

Figure 5:

Balb/c mice were treated with LPS (8mg/kg IP) to induce murine model of sepsis. Peptide P110 (0.5mg/kg IP) was administered in a subset of septic animals 3hrs following LPS treatment. (A) Illness severity and outcome quantified by change in temperature, weight, mouse sepsis score (previously published illness severity score for murine sepsis) as well as mortality. Variables evaluated every 3 hrs following LPS treatment. Temperature and weight displayed as a change from baseline (n=6 mice for control, 12 for LPS-treated mice, and 12 for LPS+P110-treated mice). (B) Change in cardiac function was measured by change in ejection fraction (EF), fractional shortening (FS) and change in velocity time integral (VTI) across the Left ventricular outflow tract. (C) Mouse sepsis score is displayed as a cumulative score per animal (n=6 control, 12=LPS, 12=LPS+P110).

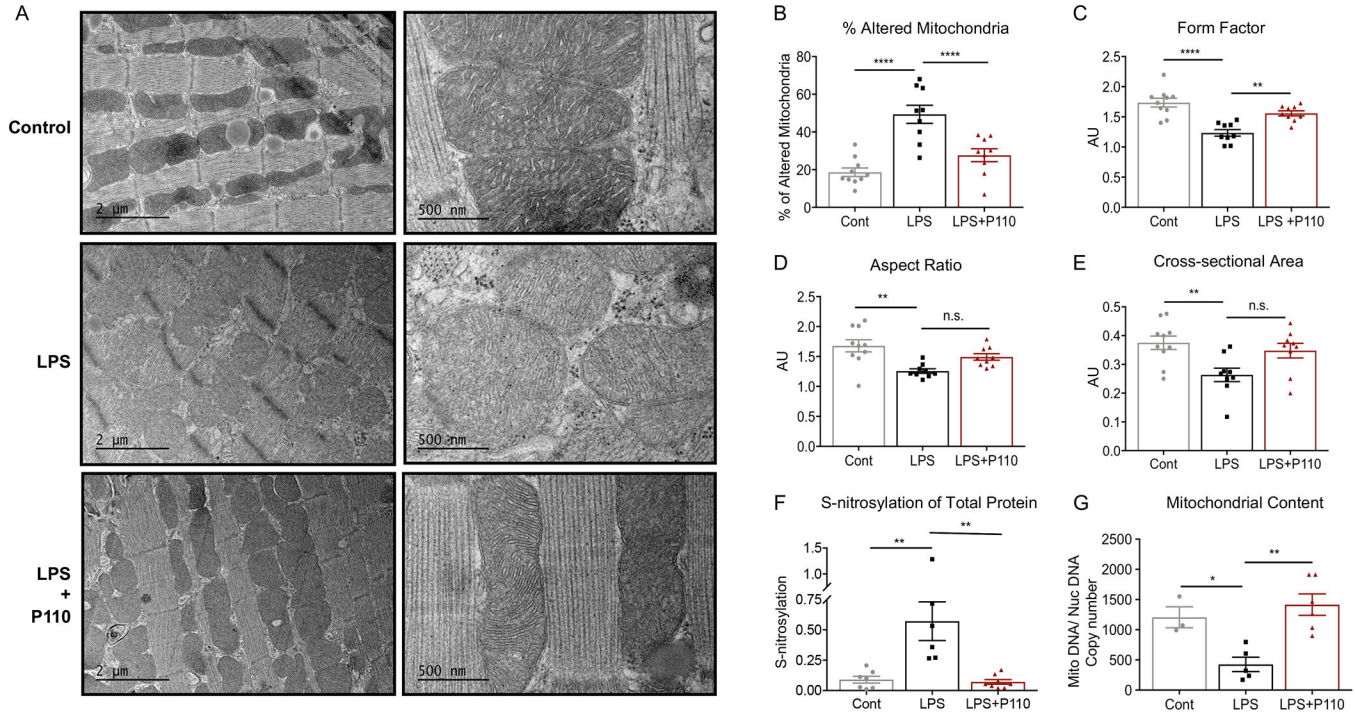

Figure 6:

(A) Electron microscopy of cardiac tissue from mice treated with control, LPS or LPS followed by P110 (n=4 per condition). Images quantified for changes in: (B) Percent altered mitochondria, (C) form factor (FF) [(perimeter^2)/(4π·surface area)], which reflects the complexity and branching aspect of mitochondria, (D) aspect ratio (AR) [(major axis)/(minor axis)], which reflects mitochondrial "length-to-width ratio", and (E) mitochondrial cross-sectional area. (F) Cardiac tissue oxidative stress was quantified by the level of oxidative post-translational modification (s-nytrosylation) proteins in the total cardiac lysates. (G) Mitochondrial content was evaluated by quantifying mitochondrial DNA as a ratio to total DNA across the three groups. Quantification and scoring done by scientist who was blinded to conditions (n=3 control mice, n=5 of LPS-treated mice and n= 5 for LPS +P110-treated mice).